Contributions to System Integration of PV and PVT Collectors with Heat Pumps in Buildings

Manuel Koch[1*] and *Ralf* Dott[1]

[1]University of Applied Sciences and Arts Northwestern Switzerland, 4132 Muttenz, Switzerland

Abstract. A common approach to improve self-consumption of photovoltaic (PV) generation in buildings with heat pumps (HP) is to overload the thermal storage capacities during times with surplus PV generation (hereinafter referred to as thermal overloading). The impact of battery capacity and domestic hot water (DHW) consumption on the effectiveness of this method in a single-family home (SFH) is evaluated through numerical simulations. Increased battery capacity is shown to decrease the effectiveness of thermal overloading. Regarding DHW consumption, temporal concentration is shown to have a stronger influence on the effectiveness of thermal overloading than total energy. Furthermore, the potential of photovoltaic-thermal collectors (PVT) as heat exchangers for air/brine/water heat pumps (ABWHP) is estimated. The results show that the properties of PVT collectors with high thermal conductivity are in the feasible range for application in a well-insulated SFH in Central European climate.

1 Introduction

Recent years have seen an increase in rooftop PV and heat pumps for residential heating [1] [2]. In addition to optimizing these components individually, the interactions between them should be examined, in order to derive guidelines for the design of building energy systems combining both. In this study, two contributions to this goal are made:

Firstly, numerical simulations are used to evaluate the effectiveness of improving self-consumption of PV generation in a SFH through thermal overloading in dependence of battery capacity and DHW consumption. Along with the increasing share of solar power in electricity generation [3], the question of electricity storage grows in significance [4] [5]. Heat pumps with control systems maximizing self-consumption of PV generation have the potential to use the thermal masses of DHW storage and the building itself to alleviate this problem, especially in buildings with underfloor heating or thermally activated building systems. This potential however depends on many parameters and boundary conditions. A realistic selection thereof is crucial for the validity of the evaluation.

Secondly, the feasibility of using PVT collectors as heat exchangers for ABWHP is estimated by comparing their thermal properties to those of dedicated heat exchangers and solar-thermal collectors. PVT collectors offer the potential to maximize energy gains from a given roof area. Compared to dedicated solar-thermal collectors, their return temperatures are often too low to be used for DHW directly. However, due to their large area, they may serve as primarily convective heat exchangers for ABWHP. If functional, this approach offers several advantages over air-source HP: The external fans of air-source HP are noisy and consume substantial amounts of electric energy. Since the PVT approach requires no fans, it emits no noise and might be more energy efficient. The first point is particularly relevant regarding the increasingly strict noise regulations in residential areas [6]. The intermediate brine cycle also allows bypassing the heat pump to recover a ground source or latent heat storage in summer.

2 Simulation Models

The simulations are conducted using Matlab/Simulink R2016b with the CARNOT Blockset Toolbox, Version 6.2. All simulations start with one month of settling time, then cover one year. For the analysis, the state of the components is sampled every minute.

2.1 System Overview

Fig. 1 and Fig. 2 show the hydraulic and electric schematics of the examined system, consisting of photovoltaics, battery, heat pump, space heating (SH), DHW storage and domestic appliances. The following sections detail the individual components.

2.2 Building

The SFH45 building as defined by IEA HPT Annex 38 SHC Task 44 [7] is used, which corresponds to a SFH meeting minimum efficiency requirements for modern buildings. The floor area is 140 m^2 with a space heating

demand of 45 kWh/m²a. The building has an underfloor heating system as well as temperature dependent ventilation and window shading, though no heat recovery for the ventilation. The internal load from occupants and household appliances is set to a constant 322 W. The implementation of the model neglects all spatial aspects and consists of two thermal masses: The heating system with 40 MJ/K and the remaining building mass with 70 MJ/K.

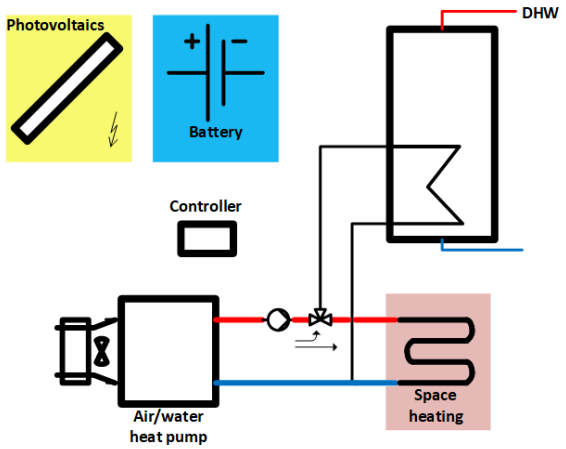

Fig. 1: Hydraulic schematic.

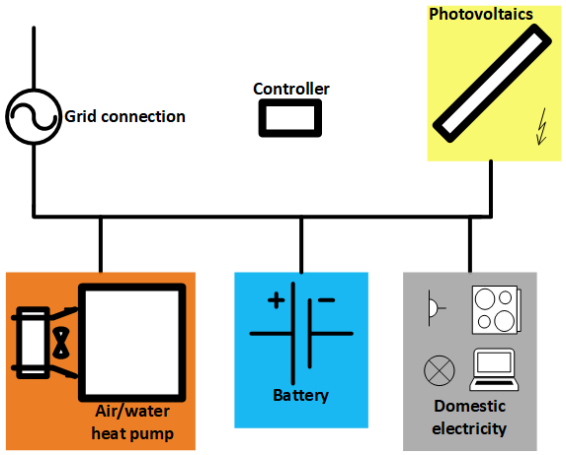

Fig. 2: Electric schematic.

2.3 Heat Pump

The building has an air/water HP with a thermal power of 6 kW at the operation point A-7/W35. The auxiliary electric heater also has a power of 6 kW. The implementation uses power maps, based on input air temperature and output water temperature. The power for defrosting the external heat exchanger is integrated into the power maps.

2.4 Domestic Hot Water Storage

The DHW storage has a capacity of 390 l and is well insulated. The heat pump is connected to a heat exchanger coil. The DHW is drawn directly from the storage. Stratification is taken into account by discretizing the storage into 10 vertical nodes.

2.5 Photovoltaics, Inverter and Battery

The building has a rooftop photovoltaic system with a peak power of 5 kW. The roof is facing south with a 30° inclination. The implementation calculates the power as an algebraic function of solar irradiance, taking cell temperature into account. The inverter is implemented as a simple power-efficiency-curve. The battery has a usable capacity of 5.9 kWh and an efficiency of 95% each way, which corresponds to the data sheet of the battery installed in the institute's laboratory. Charging the battery is always prioritized over grid feed-in and thermal overloading. Discharging the battery is always prioritized over grid draw.

2.6 Controls

The conventional control system keeps the DHW storage temperature in a defined band. The space heating supply temperature is kept in a defined band around a set point in function of the averaged ambient temperature (T_{amb}), while the room temperature is used to control the mass flow to the heating system. If the surplus PV generation is below 1500 W, the thermal overloading control is identical to the conventional control. Above this threshold, the temperature set points are elevated by 1 K for the room temperature and 7.5 K for the DHW storage. The parameters for both control strategies are listed in Table 1. The surplus PV generation is processed through a first order low-pass filter with a time constant of 600 s.

Table 1: Control parameters for both controllers in °C.

Parameter	Conventional	Overloading
	$P_{PV,surplus}$ ≤ 1500 W	$P_{PV,surplus}$ > 1500 W
$T_{SH,supply}$ at T_{amb} = -8 °C	32	32
$T_{SH,hysteresis,low}$	-1	-1
$T_{SH,hysteresis,high}$	1	1
$T_{DHW,low}$	40	47.5
$T_{DHW,high}$	50	57.5
T_{Room}	20	21

With the given temperatures, the usable thermal overloading capacities are 11.1 kWh for the heating system, 19.4 kWh for the remaining building mass and 3.4 kWh for the DHW storage. This stands in comparison to the battery capacity of 5.9 kWh, the average daily space heating load of 17.3 kWh and the average daily DHW consumption of approx. 6 kWh, depending on the DHW profile, defined in chapter 3.3.

2.7 Hydraulics

The hydraulic are highly simplified. Pipes and valves have neither dynamics nor friction. The circulation pumps feed a constant mass flow at a constant electric power when running. The power consumption of these

pumps can be thought of as a representation of the hydraulic resistance.

3 Boundary Conditions

The following boundary conditions are used for the simulations. Since the results are expected to depend strongly on the synchronicity of the conditions, they all have a one-minute resolution.

3.1 Weather

A weather data set for the city of Strasbourg, France is used. The average temperature is 11 °C and the annual solar irradiance 1102 kWh/m^2.

3.2 Domestic Electricity Consumption

A stochastic domestic electricity consumption profile with a total annual energy of 3385 kWh is used. While 90% of all loads are below 1 kW, the peak load is at 7.1 kW [8].

3.3 Domestic Hot Water Consumption

Three stochastic annual profiles and three repetitive daily profiles are used, shown in Table 2. The stochastic profiles are mostly scaled versions of each other with small differences in individual drawings. The basic repetitive profile is the "Tapping Cycle M" from the EN 13203 standard. This profile has one large drawing each in the morning and evening. Two modifications thereof are used, in which these drawings are concentrated in the morning ("M-mor") or the evening ("M-eve"). Fig. 3 compares the averaged cumulative energy of all profiles over one day. While the curves for the repetitive profiles are an exact match for every day, the stochastic profiles have large deviations between individual days [9].

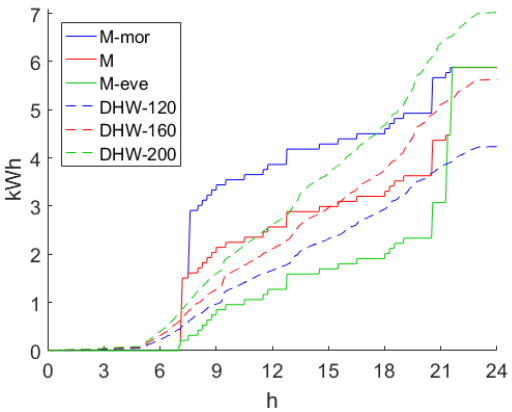

Fig. 3: Averaged cumulative energy of DHW profiles.

Table 2: DHW profiles.

Profile	Energy [kWh/d]	Notes
DHW-120	4.24	Stochastic, ~120 l/d
DHW-160	5.63	Stochastic, ~160 l/d
DHW-200	7.02	Stochastic, ~200 l/d
M-mor	5.88	Repetitive, modification based on EN 13203
M	5.88	Repetitive, from EN 13203
M-eve	5.88	Repetitive, modification based on EN 13203

4 Results

Four key performance indicators (KPI) are calculated for all simulations: Self-generation (SG), self-consumption (SC), grid feed-in (GFI) and grid draw (GD) [10].

4.1 Variation of Battery Capacity

Three battery capacities are compared. The 5.9 kWh battery corresponding to the real one is complemented by a 3.0 kWh battery and a simulation without battery (0.0 kWh). As a baseline, Table 3 shows the key performance indicators for varying battery capacity with the conventional control system. Increasing battery capacity has a significant impact on the KPI, though with a quickly diminishing marginal benefit.

Table 3: KPI at battery capacity with conventional control.

Battery capacity	SG	SC	GFI	GD
	%	%	kWh/a	kWh/a
5.9 kWh	48.8	63.9	1739	3076
3.0 kWh	41.7	54.2	2211	3501
0.0 kWh	24.4	30.4	3355	4538

Table 4 shows the relative change in KPI when switching from the conventional control system to thermal overloading. In general, the expected effects are observed. The SG and SC are increased, the GFI and GD are reduced. For the SG and SC, the impact of thermal overloading quickly diminishes with increased battery capacity. For the GFI and GD, the picture is less clear. However, all reductions in GFI are consistently larger than the reductions in GD. In general, varying the battery capacity has a far greater impact than changing the control system.

Table 4: Relative change in KPI with thermal overloading compared to conventional control.

Battery capacity	SG	SC	GFI	GD
	%	%	%	%
5.9 kWh	+2.4	+2.7	-4.7	-1.8
3.0 kWh	+5.5	+5.9	-7.0	-3.4
0.0 kWh	+12.8	+14.0	-6.1	-3.2

4.2 Variation of DHW Total Energy

Table 5 shows the KPI for DHW profiles with varying total energy. The impact on all KPI is rather small. Table 6 shows the relative changes in KPI when switching from the conventional control system to thermal overloading. Similar to the varying battery capacity, all KPI change in the expected direction. SG and SC increase, GFI and GD decrease. The degree of change is similar for all DHW profiles.

Table 5: KPI at total DHW energy with conventional control.

DHW profile	SG	SC	GFI	GD
	%	%	kWh/a	kWh/a
DHW-120	49.3	63.1	1781	2975
DHW-160	48.8	63.9	1739	3076
DHW-200	48.2	64.6	1709	3187

Table 6: Change in KPI with thermal overloading compared to conventional control.

DHW profile	SG	SC	GFI	GD
	%	%	%	%
DHW-120	+2.3	+2.5	-4.3	-1.7
DHW-160	+2.4	+2.7	-4.7	-1.8
DHW-200	+2.5	+2.8	-5.0	-1.8

4.3 Variation of DHW Timing

Table 7 shows the KPI for varying daily timing of DHW consumption. Similar to the variation of total energy, the impact of DHW timing is rather small. Table 8 shows the relative changes in KPI when switching from the conventional control system to thermal overloading. While the values are similar for the profiles with DHW consumption concentrated on the morning or evening, thermal overloading shows greater impact for the distributed DHW consumption profile "M".

Table 7: KPI at DHW timing with conventional control.

DHW profile	SG	SC	GFI	GD
	%	%	kWh/a	kWh/a
M-mor	48.4	64.5	1713	3147
M	48.1	64.2	1726	3166
M-eve	48.5	64.6	1707	3141

Table 8: Change in KPI with thermal overloading compared to conventional control.

DHW profile	SG	SC	GFI	GD
	%	%	%	%
M-mor	+1.7	+1.7	-3.0	-1.4
M	+2.9	+3.0	-5.5	-2.4
M-eve	+2.3	+2.6	-4.8	-1.6

The results for the grid interaction are summed up in Fig. 4. It can be seen that varying the timing of DHW consumption has a stronger influence on the impact of thermal overloading than varying the total energy.

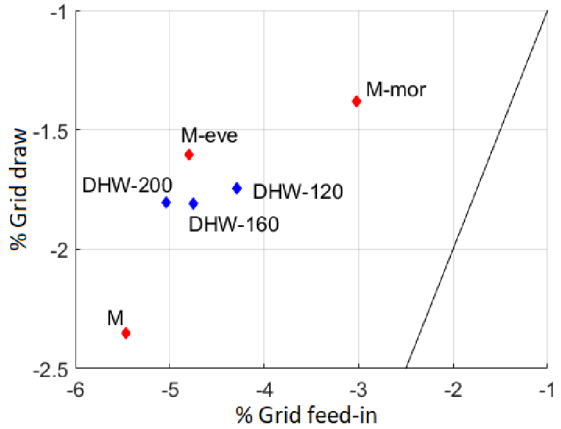

Fig. 4: Relative change in grid interaction when replacing conventional control with overloading control.

To examine the observed effects in detail, the daily surplus PV generation ($P_{el,surplus} = P_{PV} - P_{el,domestic}$) and the electric power of the heat pump with both control strategies ($P_{el,HP,conventional}$, $P_{el,HP,overloading}$) are shown in the figures below. Fig. 5 shows the results for the distributed repetitive DHW profile "M". Compared to the conventional control, the HP power with thermal overloading is clearly shifted to the midday hours with high electric surplus. The effect is most pronounced for the DHW peaks in the morning and evening.

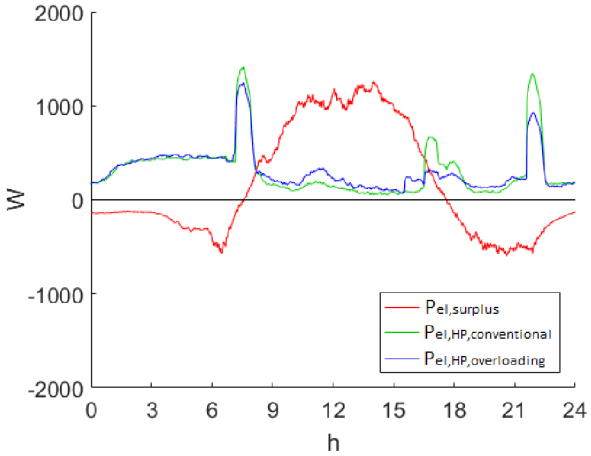

Fig. 5: Averaged daily electric power with DHW profile "M."

Fig. 6 shows the results for the repetitive DHW profile "M-mor", which has a concentration of DHW consumption in the morning. The difference between the two control strategies is much smaller with the concentrated DHW profile than with the distributed one. The high DHW consumption in the morning depletes the DHW storage, forcing a charging cycle during hours with low surplus PV generation, limiting the potential benefits of thermal overloading.

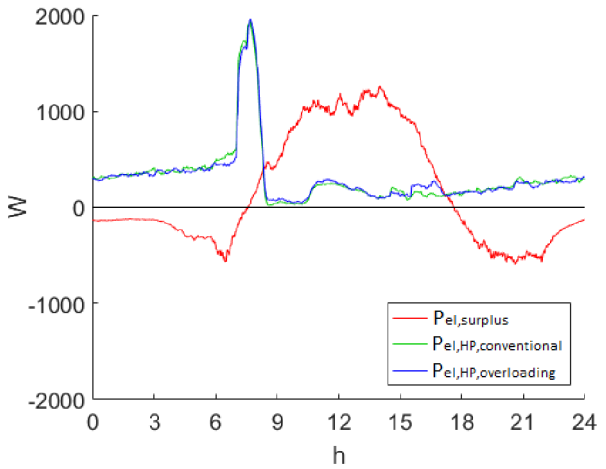

Fig. 6: Averaged daily electric power with DHW profile "M-mor."

5 PVT Collector as Heat Exchanger

With a given brine/water HP, mass flows and operating temperatures, the thermal power of the system is proportional to the UA value of the heat exchanger on the air/brine side. Three heat exchange systems on the air/brine side are compared here: Forced-air heat exchangers, PVT collectors and uncovered solar-thermal collectors. Fig. 7 shows the simplified hydraulics of an air/brine/water PVT-HP system.

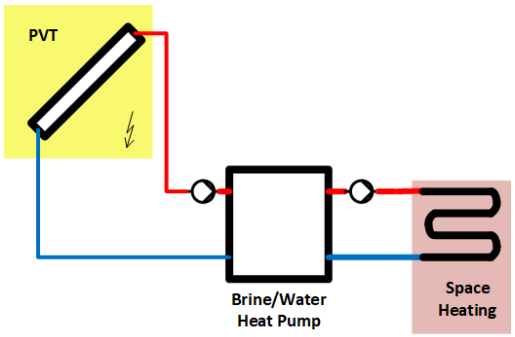

Fig. 7: Simplified hydraulic schematic of a PVT-HP system.

In a series of measurements, the UA value of an air/brine heat exchanger supplying a brine/water HP with a thermal power of 6 kW at the operating point A-7/W35 is determined to be 1500 W/K, corresponding to 250 W/K per kW of heating power. This value is compared to the wind-dependent UA values for PVT collectors, according to equation (1), where u is the wind speed and A is the heat exchanger area. Solar irradiance is neglected, since it is considered a minor factor during the critical winter months [12].

Table 9 shows the corresponding parameters for a PVT collector with high thermal conductivity, a PVT collector with average thermal conductivity and a purely solar-thermal air/brine pipe heat exchanger, consisting of two rows of parallel uncovered plastic pipes.

$$UA = \dot{Q}/\Delta T = (\mathrm{b}_1 + \mathrm{b}_2 u)\mathrm{A} \qquad (1)$$

Table 9: Parameters of PVT collectors and pipe heat exchanger.

Collector	Thermal conductivity	Wind-dependent thermal conductivity
	b_1 [W/m^{2}K]	b_2 [Ws/m^{3}K]
TÜV HTC [11]	21.5	3.66
ISFH PVT-A [11]	10.2	1.15
Pipe heat exchanger [12]	27.5	47.1

Assuming a required thermal conductivity of 250 W/K per kW of heating power, the required PVT collector area is calculated using equation (1) and shown in Fig. 8. A significant difference between the three components can be seen, especially at higher wind speeds. The average wind speed from the weather data for Strasbourg is approx. 3 m/s for all seasons. The wind speed at the roof of a SFH in a built environment is estimated to be half the unimpeded speed, i.e. 1.5 m/s. With this assumption, the highly conductive PVT collectors would require an area of approx. 10 m^2 per kW of heating power. This value is in the feasible range for application in a SFH with state-of-the-art thermal insulation. E.g. 5 kW of heating power with 50 m^2 of south-facing roof area.

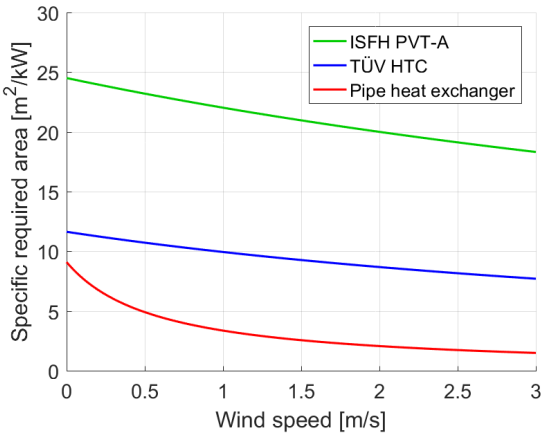

Fig. 8: Specific required PVT area per kW heating power.

Fig. 9 shows the different construction of PVT modules with high and low thermal conductivity. The difference is primarily in the insulation, consisting of an air-filled gap between the PV module and the glass cover in the front and a layer of insulating material in the back.

Fig. 10 compares the UA values of the two PVT collectors with an area of 50 m^2, the pipe heat exchanger with an area of 10 m^2 and the originally evaluated heat exchanger of an ABWHP. The 50 m^2 for the PVT collectors correspond to the south-facing roof area of the SFH45. The 10 m^2 for the pipe heat exchanger are based on a model from a predecessor study, where the remaining 40 m^2 of roof area are covered with conventional PV modules [12]. With these areas and the assumed wind speed of 1.5 m/s, the HP heat exchanger has the highest UA value, followed by the highly

conductive PVT collectors and the pipe heat exchanger. At wind speeds above 3 m/s, this relationship is inverted.

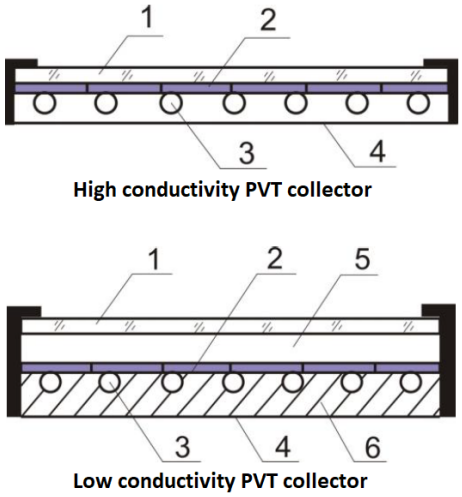

Fig. 9: Construction of PVT collectors. (1) Glass cover (2) PV module (3) Piping (4) Back cover (5) Air gap (6) Thermal insulation [11]

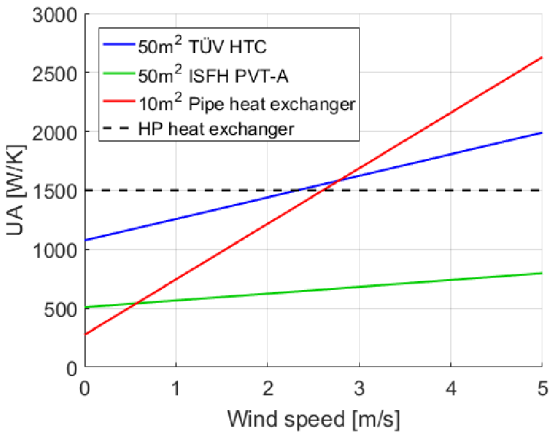

Fig. 10: UA values for PVT collectors and pipe heat exchanger at given area. Comparison with HP heat exchanger.

6 Discussion

While the results for varying battery capacity yield no surprises, the parameters correspond to new batteries in good condition. As capacity and efficiency decrease with age, the results may change. DHW consumption patterns have many characteristics: Total energy, repetitiveness, daily timing, concentration respectively distribution of drawings, etc. The significance of the results may be improved by using additional DHW profiles covering all these aspects. Varying the DHW storage capacity may also yield additional insights. For both evaluations, it should be noted that the parameters for the thermal overloading have not been varied or optimized.

While the application of PVT collectors as heat exchangers for heat pumps is deemed feasible, the impact of snowfall and frosting is neglected at this point. An extended evaluation would also include a comparison of cost and efficiency with a more conventional combination of pure photovoltaics and an air-source HP.

7 Conclusions

The simulation results indicate that the potential for improving SC through thermal overloading in a SFH is rather limited. In comparison, the impact of a medium capacity battery is much higher. The addition of a battery also further lowers the benefits of thermal overloading. The variation of DHW consumption patterns are of comparable significance to the potential of thermal overloading. However, temporal concentration respectively distribution of DHW consumption has a greater impact than its total energy. This effect may be even stronger with lower DHW storage capacity. The relationship between optimal SC of PV generation and DHW storage capacity should be kept in mind when applying legionella counter-measures, which often involve minimizing the volume of standing hot water.

The application of PVT collectors as heat exchangers for heat pumps appears to be feasible for a well-insulated SFH with a relatively large usable roof area. It is however crucial to use PVT collectors designed for high thermal conductivity, since solar-thermal systems used as source for a heat pump gain most heat from convection, not solar irradiance [12].

8 Outlook

The evaluation of the influence of DHW consumption patterns may be extended with additional DHW profiles and different DHW storage capacities. An experimental evaluation of an energy management system (EMS) to complement the simulations is currently in progress. Fig. 11 shows a preliminary measurement. The regular temperature band for the DHW storage is 40-50 °C. During the afternoon hours with surplus PV generation ($P_{el,surplus} = P_{PV} - P_{el,domestic} - P_{battery} - P_{el,HP,DHW}$), the EMS triggers a DHW charging cycle ($P_{el,HP,DHW}$) before the lower temperature limit is reached and overloads the storage to approx. 54 °C (T_{DHW}). The temperature dip before the charging is the result of turbulences stirring up the stratified layers of water. Compared to the identical test without the EMS, the SC and SG are significantly increased while the GFI and GD are significantly decreased. Extended results may be published in a few months.

The evaluation of PVT collectors yields positive indicators and may be continued with simulations and experiments. In addition to the heating application, PVT collectors could also be used for cooling. Their large upward facing surface and high infrared emissivity makes them suitable for nocturnal radiative cooling. While this approach is already being investigated, the cooling power per surface area is usually rather low [13] [14]. A heat pump elevating the collector temperature during cooling operation could counter this limitation.

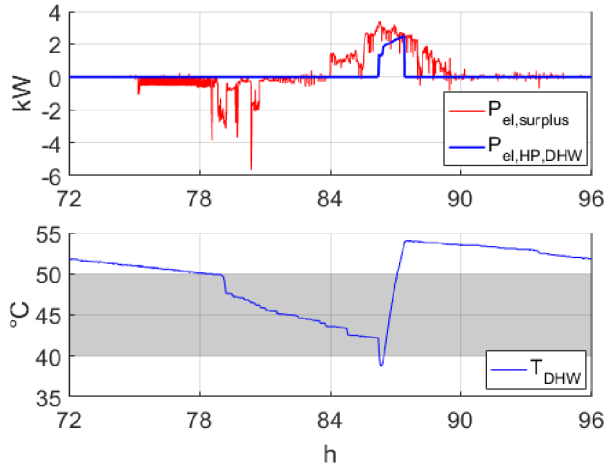

Fig. 11: Surplus PV generation without DHW charging, electric power for DHW charging and DHW storage temperature.

References

1. "Heat pump sales overview," EHPA, www.stats.ehpa.org/hp_sales/story_sales/, retrieved 30th of Oct, 2018
2. "Statistik 2017," FWS, https://www.fws.ch/wp-content/uploads/2018/05/FWS_Statistiken_2017_V2.pdf, retrieved 30th of Oct, 2018
3. "Energieversorgung der Schweiz und internationale Entwicklung," UVEK, CHE, 2017
4. "Grid Energy Storage," U.S. Department of Energy, USA, 2013
5. "U.S. Battery Storage Market Trends," U.S. Department of Energy, USA, 2018
6. "Lärmschutz-Verordnung 814.41, Stand am 1. April 2018," Bundesgesetz, CHE, 2018
7. R. Dott, M.Y. Haller, J. Ruschenburg, F. Ochs and J. Bony, "The Reference Framework for System Simulations of the IEA SHC Task 44 / HPP Annex 38, Part B: Buildings and Space Heat Load, A technical report of subtask C, Report C1 Part B," FHNW, CHE, 2013.
8. N. Pflugradt, "LoadProfileGenerator," TU Chemnitz, https://www.loadprofilegenerator.de/
9. "DHWcalc," Universität Kassel, https://www.uni-kassel.de/maschinenbau/institute/ite/fachgebieteleitung/solar-und-anlagentechnik/downloads.html
10. C. Finck, P. Beagon, J Clauss, T. Péan, P. Vogler-Finck, K. Zhang and H. Kazami, "Review of applied and test control possibilities for energy flexibility in buildings," IEA EBC Annex 67, 2018
11. M. Adam, H.P. Wirth and R. Radosavljevic, "Verbundprojekt: Standardisierung und Normung von multifunktionalen PVT Solarkollektoren (PVT-Norm), Teilvorhaben: PVT-System-anwendungen und Simulationen," FH Düsseldorf, DEU, 2015
12. R. Dott, T. Afjei, C. Winteler and A. Genkinger, "SOFOWA : Kombination von Solarthermie, Fotovoltaik, Wärmepumpen und Eisspeicher," FHNW, CHE, 2016
13. U. Eicker and A. Dalibard, "Photovoltaic-thermal collectors for night radiative cooling of buildings," Solar Energy, vol. 85, pp. 1322-1335, 2011
14. A. Amir and R. van Hout, "A transient model for optimizing a hybrid nocturnal sky radiation cooling system," Renewable Energy, vol. 132, pp. 370-380, 2019 (in press)